

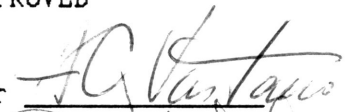
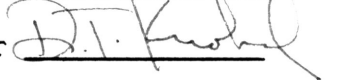
SEA-TRUTHING A SATELLITE TECHNIQUE  
FOR OCEAN SURFACE FLOW ESTIMATION

Charlie Nelms Barron Jr.  
University Undergraduate Fellow, 1989-90  
Texas A&M University  
Department of Oceanography

APPROVED

Fellows Advisor

Honors Director

## CONTENTS

	Page
FIGURES AND TABLES . . . . .	iii
ABSTRACT . . . . .	v
SEA-TRUTHING A SATELLITE TECHNIQUE FOR OCEAN SURFACE FLOW ESTIMATION	
INTRODUCTION . . . . .	1
Why Do We Need to Estimate Ocean Surface Flow? . . . . .	1
Why Use Satellite Methods to Estimate Ocean Surface Flow? . . . . .	1
What Kind of Satellite Data Is Used Here? . . . . .	3
How Is Surface Flow Estimated from AVHRR Images? . . . . .	4
What Is the Purpose of this Paper? . . . . .	5
How Does the Sea-Truthing Proceed? . . . . .	6
DATA . . . . .	6
AVHRR Images . . . . .	6
Drifting Buoys . . . . .	10
DATA PROCESSING . . . . .	12
Parcel Mover . . . . .	12
Flow Fields . . . . .	13
SEA-TRUTHING . . . . .	15
RESULTS AND CONCLUSION . . . . .	17
REFERENCES . . . . .	28
APPENDIX A . . . . .	29
APPENDIX B . . . . .	30

## FIGURES AND TABLES

Figure	Page
1a. NOAA 10 AVHRR images March 10, 14:23 and March 11, 14:00 . . .	8
1b. NOAA 11 AVHRR images March 11, 08:47 and March 12, 08:37 . . .	9
2. USCG drifters in northwestern Gulf of Mexico . . . . .	11
3a. Vectors derived from AVHRR feature tracking between images of Julian days 69 14:23 and 70 14:00 . . . . .	14
3b. Vectors derived from AVHRR feature tracking between images of Julian days 70 08:47 and 71 08:37 . . . . .	14
4. Actual 2-day track of USCG 4571 and 5 model parcels. Vectors day 69:14 - 70:14. Parcels start day 69:14. . . . .	20
5. Actual 2-day track of USCG 4573 and 5 model parcels. Vectors day 69:14 - 70:14. Parcels start day 69:14. . . . .	20
6. Actual 2-day track of USCG 4574 and 5 model parcels. Vectors day 69:14 - 70:14. Parcels start day 69:14. . . . .	21
7. Actual 2-day track of USCG 4571 and 5 model parcels. Vectors day 70:08 - 71:08. Parcels start day 70:08. . . . .	21
8. Actual 2-day track of USCG 4573 and 5 model parcels. Vectors day 70:08 - 71:08. Parcels start day 70:08. . . . .	22
9. Actual 2-day track of USCG 4574 and 5 model parcels. Vectors day 70:08 - 71:08. Parcels start day 70:08. . . . .	22
10. Actual 2-day track of USCG 4571 and 5 model parcels. Vectors day 69:14 - 70:14. Parcels start day 69:02. . . . .	23
11. Actual 2-day track of USCG 4573 and 5 model parcels. Vectors day 69:14 - 70:14. Parcels start day 69:02. . . . .	23
12. Actual 2-day track of USCG 4571 and 5 model parcels. Vectors day 70:08 - 71:08. Parcels start day 69:20. . . . .	24
13. Actual 2-day track of USCG 4573 and 5 model parcels. Vectors day 70:08 - 71:08. Parcels start day 69:20. . . . .	24
14. Actual 2-day track of USCG 4574 and 5 model parcels. Vectors day 70:08 - 71:08. Parcels start day 69:20. . . . .	25

Figure	Page
15. Position difference between parcel and buoy vs. time. Vectors day 69:14 - 70:14. Parcels start day 69:14. . . . .	26
16. Position difference between parcel and buoy vs. time. Vectors day 70:08 - 71:08. Parcels start day 70:08. . . . .	26
17. Position difference between parcel and buoy vs. time. Vectors day 69:14 - 70:14. Parcels start day 69:02. . . . .	27
18. Position difference between parcel and buoy vs. time. Vectors day 70:08 - 71:08. Parcels start day 69:20. . . . .	27
Table	Page
A1. Drifting Buoy Initial and Final Times and Positions . . . . .	29
B1. RMS distance between model parcels and actual buoys . . . . .	30

## ABSTRACT

Feature tracking is a technique that produces a sea surface velocity field from sequential images of sea surface brightness temperature derived from satellite measurements of upwelling radiation intensity. To test the validity of the vector fields produced by feature tracking, the trajectories of model water parcels moved by the vector field are compared with the trajectories of actual drifting buoys. Six buoys in the Gulf of Mexico during the spring of 1989 serve as the basis for the comparison. Using feature tracking on two different image pairs I estimated two velocity vector fields. I then developed and used a fourth-order Runge-Kutta integration routine to move model water parcels through the field, using derivatives supplied by bivariate interpolation directly from the velocity field. The correlation between parcel and buoy tracks is fairly good over the first 24 hours, although the results show wide variability and indicate a direction for improvement. Increased proficiency in feature tracking, advancement to time-dependent fields, and improved interpolation methods would allow vector fields derived by feature tracking to more closely mirror kilometer scale sea surface motion.

## INTRODUCTION

### Why Do We Need to Estimate Ocean Surface Flow?

On March 24, 1989, millions of gallons of oil began to spill from the grounded Exxon Valdez and spread over Alaska's Prince William Sound. The Valdez spill, one of the worst ecological disasters ever to occur in North America, demonstrated the insufficiency of oil spill containment procedures to cope with major accidents. To better deal with oil spills in the future, response teams must be able to quickly and accurately determine where the oil is going; they must estimate sea surface flow in the region of the accident. In the past, historical data has been used to tabulate average surface currents into one-degree latitude-longitude boxes. However, this method gives unacceptable spatial resolution and unreliable results [Vukovich, 1984]. In some instances, actual surface flow is quite different from the historical average for the same region. Reliable estimation of surface flow is vital not only to oil spill containment but also to other activities ranging from air-sea rescue to shrimp harvest predictions. Clearly, oceanographers need a generally applicable, easily executable method to estimate ocean surface flow.

### Why Use Satellite Methods to Estimate Ocean Surface Flow?

Ocean surface flow may be measured in a variety of ways. Moored current meters, tracked drifting buoys, arrays of salinity and temperature versus depth, shipboard doppler acoustic log, and other sources can provide information about water motion. Some other methods employ information acquired by satellite-carried instruments to reveal the movement of the water. Although satellite methods of estimating

ocean surface flow have some disadvantages, several inherent advantages make satellite-based techniques an attractive option.

Satellite methods of estimating sea surface flow have some disadvantages. Satellites provide poor small scale resolution because of their high altitude. Cloud cover and other atmospheric interference often obscures and may eliminate periods of data. The initial cost incurred to place a satellite into orbit is expensive. Uncertainty in satellite data increases for regions of increasing distance from nadir, the line on the globe directly underneath the satellite. The satellite data used in this study is based on measurements of upwelling infrared radiation. Since satellite-based infrared sensors receive thermal radiation only from the uppermost millimeter of the ocean, the images provide no information on changes in deeper water. Motion is estimated by tracking displacement of temperature features, so the method evaluated in this paper works poorly in water with relatively uniform surface temperature.

However, satellite methods of determining ocean surface flow offer some advantages that are unmatched by other sources. Each day, satellites collect data from every area on the globe. The odds are very slim that the next major oil spill will occur over an array of current meters or during a nearby oceanographic cruise. Yet satellites making oceanographic measurements will have already provided the information needed to predict the movement of the oil slick. Since satellites sweep across a large area in a relatively short time, satellite data is very nearly synoptic, that is, satellites provide a comprehensive view of the region of interest as it exists at a single time. While a ship might

take several days to make sufficient measurements to cover a large eddy, satellites cover it so quickly that its initial and final readings are virtually simultaneous. Satellites offer the most feasible means to view large areas and mid-ocean regions. Finally, satellites provide an easy means of gathering data, especially compared to the work required to put together an oceanographic cruise. Because satellites offer so many valuable advantages, oceanographers should develop ways to use their remote sensing capabilities in oceanographic research.

#### What Kind of Satellite Data Is Used Here?

This paper examines a technique which uses data from satellite-carried advanced very high resolution radiometer (AVHRR). Today AVHRR operates aboard two National Oceanic and Atmospheric Administration (NOAA) satellites, NOAA 10 and NOAA 11; AVHRR has been carried on all satellites in the NOAA series since NOAA 6. NOAA 10 and NOAA 11 are polar orbiters with a phase difference of about 90 degrees, so the time between the passing of NOAA 10 and the appearance of NOAA 11 over a region is about 6 hours. The orbit paths make an angle of 23 degrees with the equator to minimize the effect of solar glare from the oceans.

A passive instrument, the AVHRR measures the intensity of upwelling radiation in various band widths or channels. The radiometer scans back and forth over lines perpendicular to its path, completing 360 lines per minute. Each line consists of 2048 samples, where each sample is approximately a 1.1 km x 1.1 km pixel. Because samples on the edges of



the lines encompass more area than the samples near nadir, samples on the edges are less reliable.

The various channels of the AVHRR view windows of radiation that are least influenced by atmospheric absorption. Channel 4, a mid infrared channel, detects the intensity of radiation with wavelength between 10.5 microns and 12.5 microns. By comparing the intensity of channel 4 upwelling radiation with the radiation expected from a black body, one may calculate the brightness temperature, an estimate the sea surface temperature of the sample. Often channel 5 is combined with channel 4 to produce more precise temperature readings. However, this paper evaluates a surface flow estimation procedure which uses only channel 4 AVHRR. Combining channels obscures gradients, and since the method evaluated here tracks movement of brightness temperature features, the gradients should be as sharp as possible.

#### How Is Surface Flow Estimated from AVHRR Images?

Several methods have been developed to estimate surface flow fields from AVHRR images. The techniques generally estimate velocity either by tracking features in the brightness temperature between sequential images or by processing the image under various physical constraints (Kelly, 1988). Vukovich (1984) derived sea surface temperature distributions from single AVHRR images and related them to surface salinity (Molinari, et al, 1976). Given the temperature and salinity, Vukovich calculated density (Eckart, 1958) and from the density gradient calculated the geostrophic current. Emery, et al (1986) objectively tracked water between sequential images by converting the AVHRR images

into images of sea surface temperature gradient and then locating the maximum correlation of 22 by 22 pixel sections of the first image with 32 by 32 pixel sections of the second image.

This paper examines a technique called feature tracking, a technique of interactively tracking brightness temperature features between sequential AVHRR images. This method was presented by Vastano and Borders (1984) and extended by Vastano and Reid (1985). The method utilizes a pair of AVHRR channel 4 images separated by about 24 hours. By flickering back and forth between the images on a high resolution monitor, the investigator interactively determines the displacement of temperature patterns and indicates the displacement with a vector. The velocity is then the displacement vector divided by the time between the images. This method generates a nonuniformly distributed flow field capable of velocity resolution down to a few kilometers/day. Since the investigator subjectively determines feature displacement, vector fields are somewhat irreproducible; another investigator repeating the same procedure would see slightly different displacements and hence would produce a slightly different vector field.

#### What Is the Purpose of this Paper?

The purpose of this paper is to present the results of an effort to sea-truth velocity vectors derived using feature tracking. To sea-truth means to compare the results derived from the estimation with actual events which occurred in the sea; in this case, sea-truthing means comparing trajectories of model water parcels moved by the estimated

velocity fields with the satellite-tracked trajectories of real drifting buoys drogued to 2.7 meters.

#### How Does the Sea-Truthing Proceed?

The procedure of sea-truthing consists of four stages. The first step is selecting and processing the buoy data set which will serve as a reference. The raw buoy latitude and longitude fixes are fitted by cubic splines, to provide buoy position at any instant. The second step is creating the water parcel model, a model which uses the velocity vectors produced in the feature tracking to move model water parcels inserted at locations on the actual buoy tracks. The third step is selecting and processing the AVHRR images, producing the velocity vector fields using feature tracking. The final step is projecting the motion of the model water parcels on the days of the vector fields and comparing the model trajectory with the actual trajectory.

### DATA

#### AVHRR Images

The AVHRR image data base available for this study covered the Gulf of Mexico from March 6 to April 30. However, clouds obscured the upwelling radiation in many of the images; some images were rendered completely unusable. Usable images were navigated and registered to a Mercator projection with an uncertainty of 1 km. The patterns of infrared radiation intensity were then converted into sea surface brightness temperature distributions, but no correction was made for atmospheric interference. The absolute water temperatures in the images

were not important, only the differences. For the actual feature tracking, I used 512 pixel by 512 pixel images that had been sectioned out of the original swath of data. All of the buoys did not fit into a single 512 by 512 image, so I concentrated on the northwestern corner of the Gulf of Mexico, an area which contained most of the buoy trajectories. I selected March 10 to March 12 as the ideal window for the study; the images were clear, features were sharp, and three buoy tracks were available.

The first pair of images (Figure 1a) is from the NOAA 10 AVHRR. The first image is March 10 at 14:23 while the second is 23 hours, 37 minutes later. The images are shown in a banded enhancement, an enhancement which reveals gradients well but offers no correlation between color and temperature. Clouds interfere with the southern portions of the first image but the area containing buoys is clear.

The AVHRR aboard NOAA 11 provides the second image pair (Figure 1b). The images are separated by 23 hours, 50 minutes, with the first image beginning at 08:47 on March 11. These images exhibit a linear enhancement, in which darker color represent warmer water and lighter colors reflect cooler water. In practice, I used a linear enhancement on the images while tracking features. To produce the maximum contrast of the features, I refit each linear enhancement to the subset of sea surface temperatures in the smaller viewing areas used for tracking.

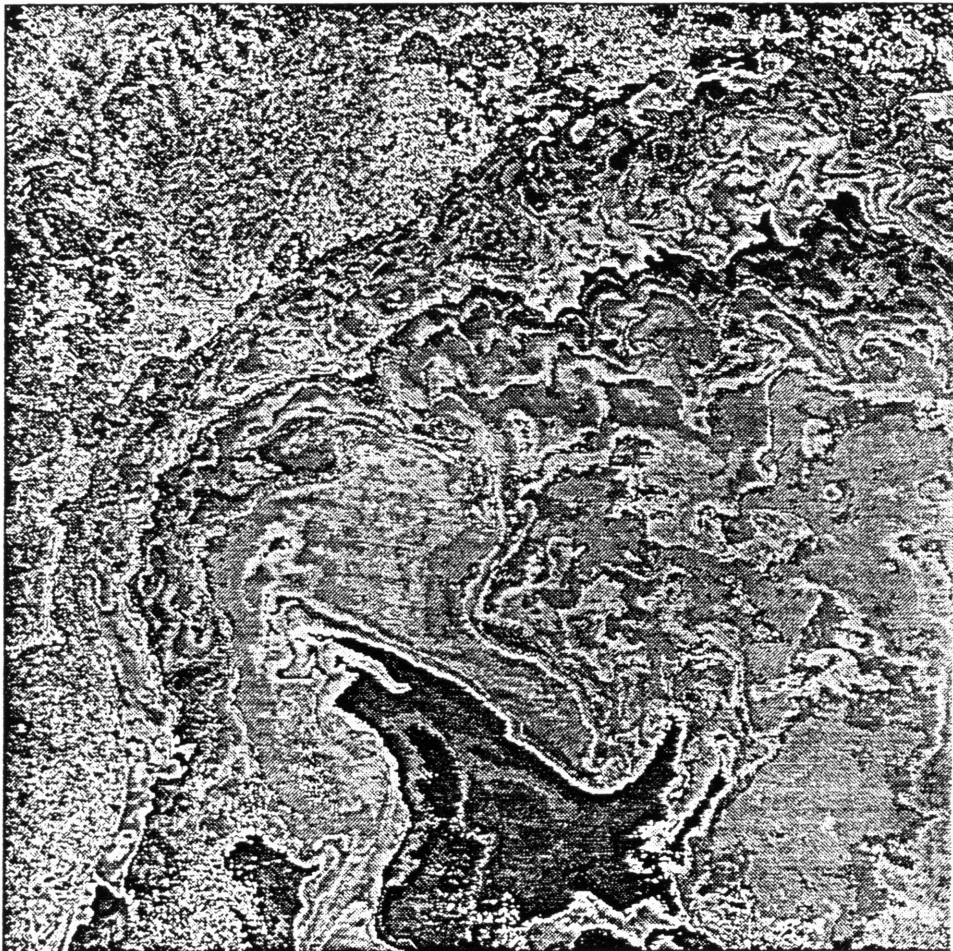
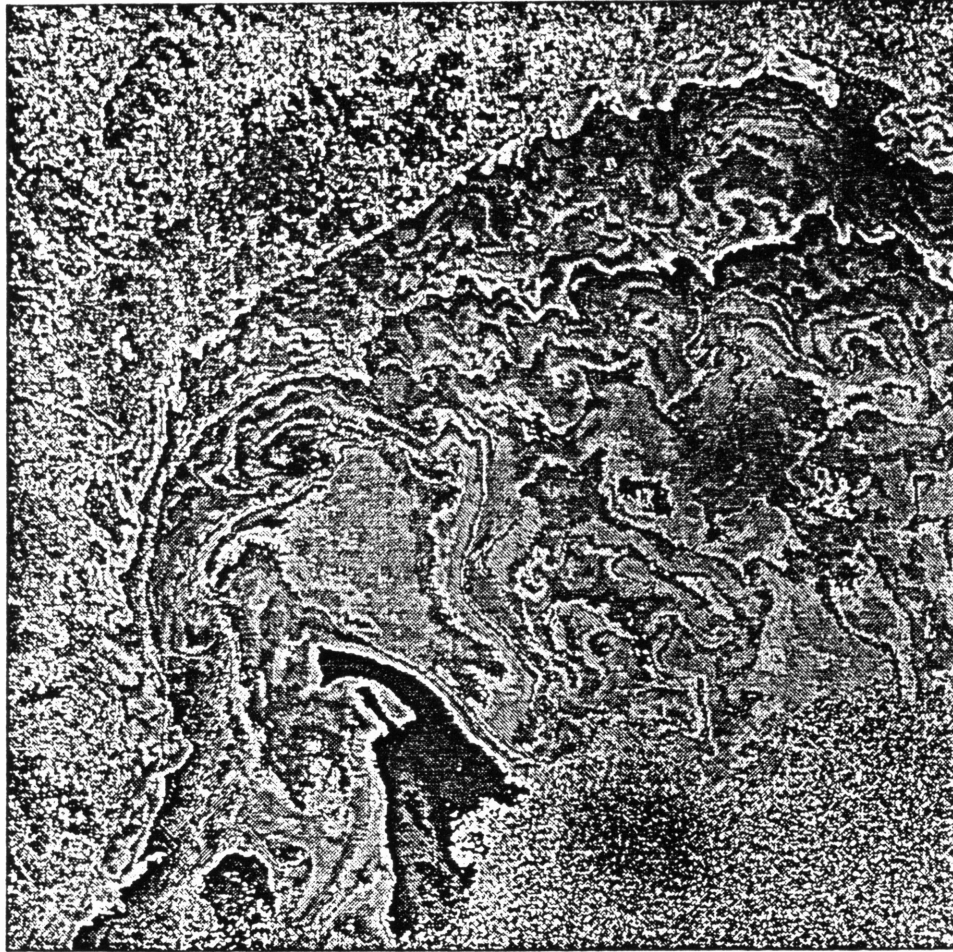


FIG. 1a. NOAA-10 AVHRR images shown in repeating band enhancement.  
top: March 10, 14:23 GMT bottom: March 11, 14:00 GMT

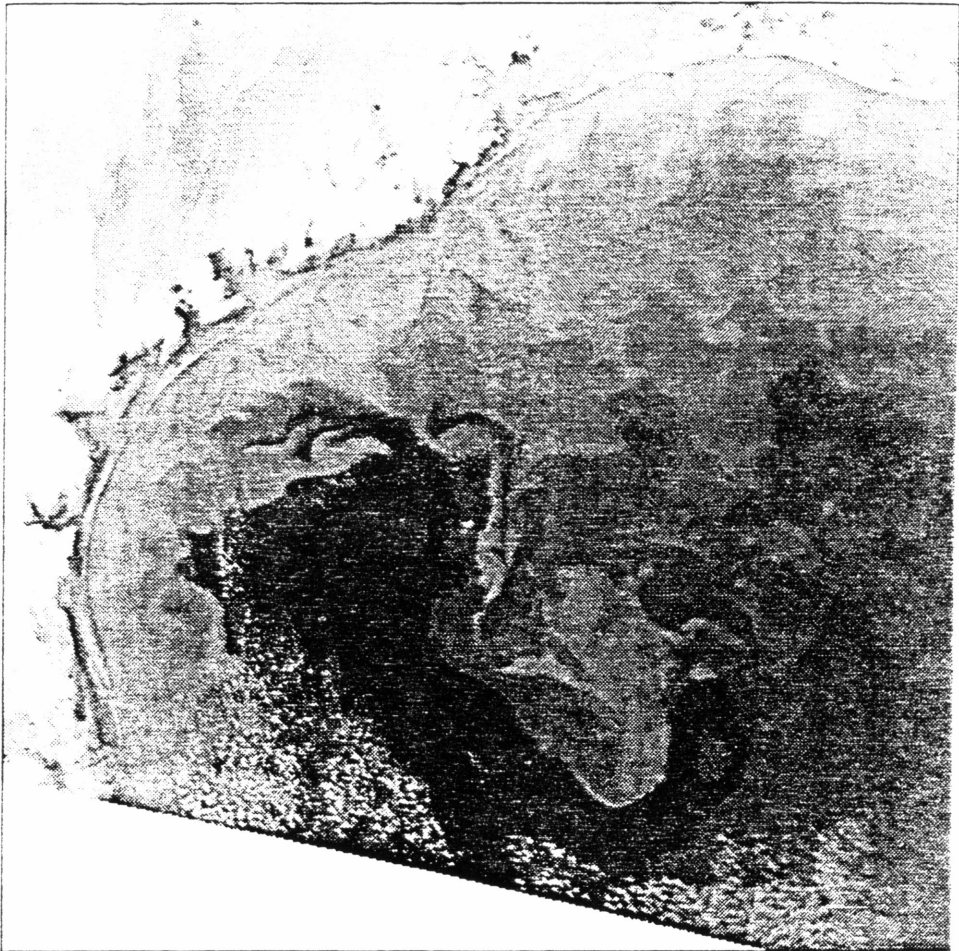
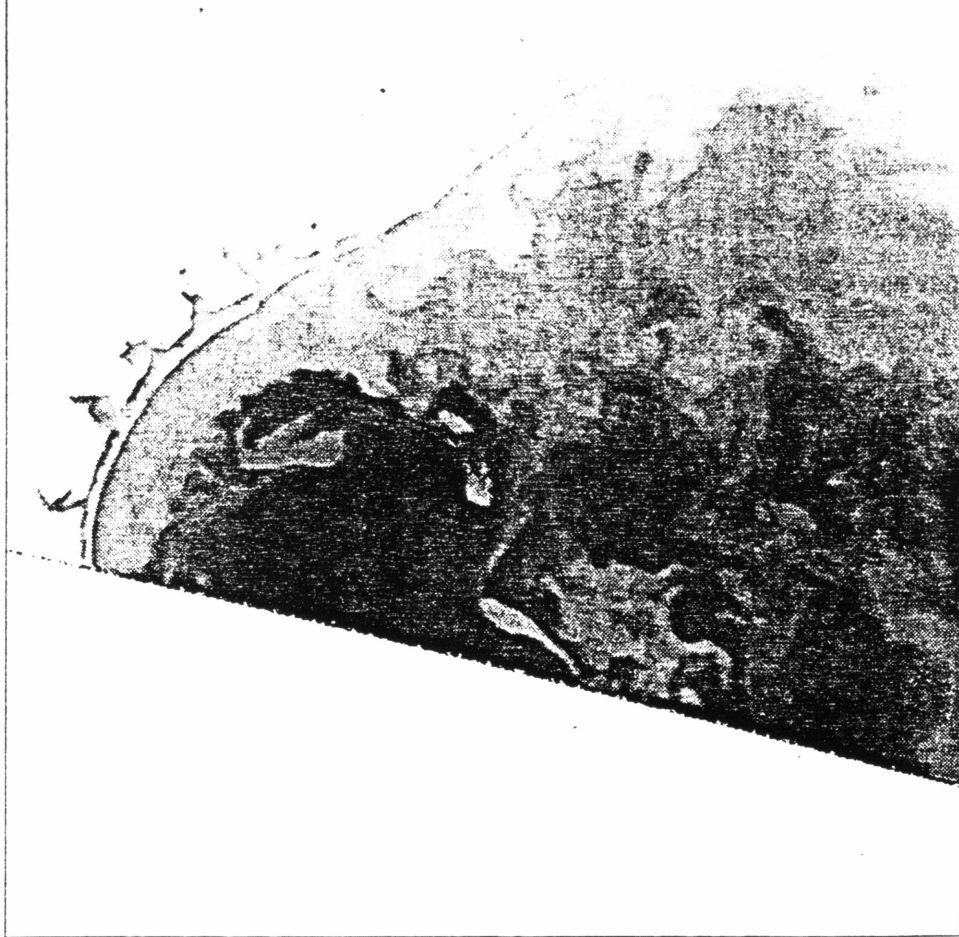


FIG. 1b. NOAA 11 AVHRR images shown in continuous linear enhancement.  
top: March 11, 08:47 GMT    bottom: March 12, 08:37 GMT

## Drifting Buoys

A set of six United States Coast Guard (USCG) drifting buoys deployed over the Texas-Louisiana shelf during March 1989 serves as the reference for the sea-truthing. Figure 2 indicates the complete buoy record and the buoy positions on March 10 through March 12, the period of this study. The drifters were launched by USCG aircraft and Texas A&M University's R/V GYRE. Information on the initial and final positions of the buoys appears in Appendix A, Table A1. Five of the buoys grounded, and two were recovered and redeployed during the eight weeks of the tracking. Satellite-based ARGOS reported the positions these shallow-drogued (2.7m) buoys and made 4 to 8 fixes per day with uncertainty of about 500m. Only three of the buoys fell within the spatial window during the two days of the image pairs selected for the sea-truthing, so much more reference track is available for other independent comparisons.

To provide a source of buoy locations at convenient times, I fit the time series of buoy latitudes and longitudes with cubic splines. By using the spline subroutines in the National Center for Atmospheric Research (NCAR) software package, the buoy position and velocity could be calculated anywhere along the trajectory easily and accurately. The spline fit also smoothed the track of the buoy, thereby removing from the buoy trajectories some of the effects of random noise due the uncertainty of the ARGOS fixes.

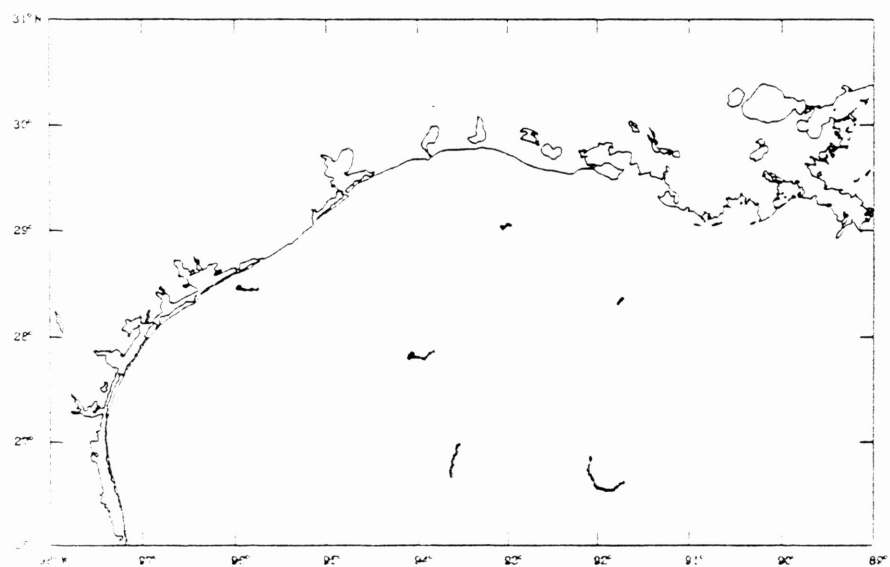
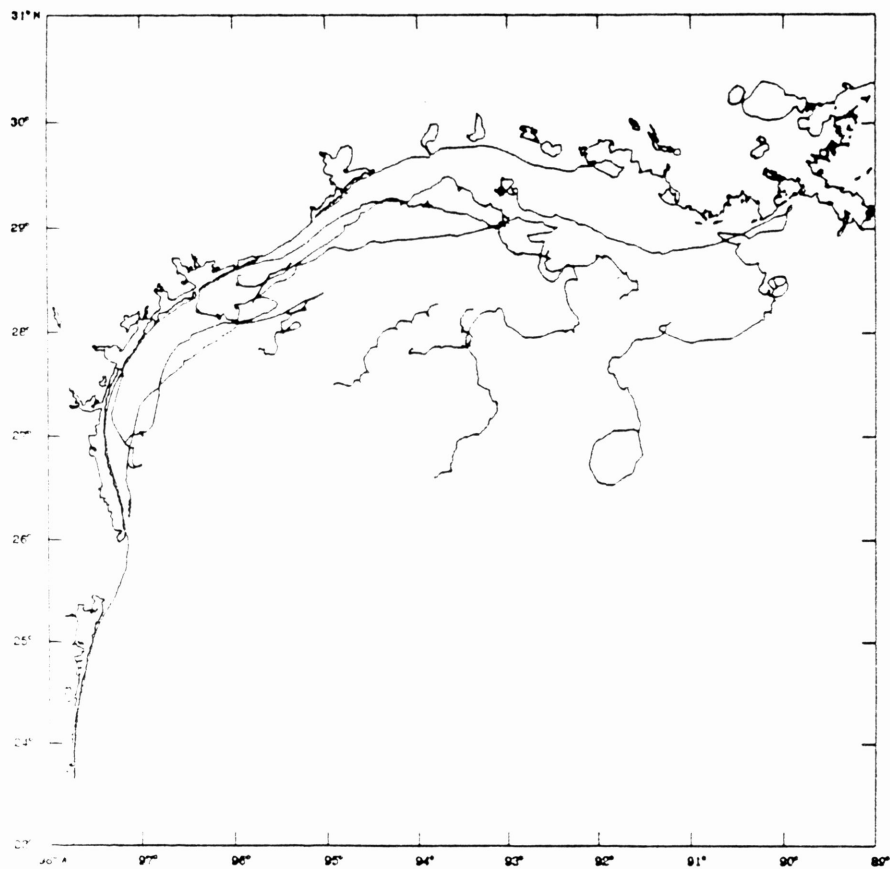


FIG. 2. USCG drifters in northwestern Gulf of Mexico during spring 1989. top: complete record bottom: March 10 - March 12



## DATA PROCESSING

## Parcel Mover

To test the reliability of velocity fields developed by the parcel tracking technique, I developed a model which uses the vectors to move a tracer or parcel through any velocity field. In this model, a parcel is inserted into a velocity field at any specified time and location. The parcel is then moved in a sequence of short time steps with velocity interpolated from the surrounding field to the parcel location. By recording each intermediate parcel position, the trajectory of the model water parcel can be compared with actual buoy trajectories.

I used a fourth-order Runge-Kutta formula to integrate the model trajectory. The Runge-Kutta formula is similar in concept to the Euler method: derivatives are evaluated at a point and the particle is then moved at that velocity for a short time interval. Repetition of this process computes the integral. The Runge-Kutta method differs from the Euler method in that four derivatives, rather than a single derivative, are computed for each time step of length  $h$ . One derivative is computed at the starting point, two are computed at estimated midpoints, and a fourth is computed at an estimated endpoint.

$$d1 = h * f'(t(n), x(n), y(n)) \quad (1)$$

$$d2 = h * f'(t(n)+h/2, x(n)+d1/2, y(n)) \quad (2)$$

$$d3 = h * f'(t(n)+h/2, x(n)+d2/2, y(n)) \quad (3)$$

$$d4 = h * f'(t(n)+h, x(n)+d3, y(n)) \quad (4)$$

A suitably chosen linear combination of these derivatives

$$x(n+1) = x(n) + (d1/6) + (d2/3) + (d3/3) + (d4/6) + O(h**5) \quad (5)$$

eliminates errors of order less than fifth. A similar calculation is performed for  $y(t)$ . Numerical Recipes (Press, et al, 1986) contains a more detailed explanation of the theory and the implementation of the Runge-Kutta method.

I calculated the derivatives by interpolating from the nonuniformly scattered velocity vectors to a velocity at the point of interest. Although I never found a two-dimensional interpolator that was completely satisfactory, I settled on bivariate interpolation routine developed by Akima (1975). Interpolation from vectors located on a regular grid produces more reliable results.

Although the Runge-Kutta method is suitable for a time-dependent field, the fields I am using are time-independent. Given more time I would combine vector fields into a time-dependent series. A time-dependent flow field is physically more realistic and would produce a more accurate model trajectory.

#### Flow Fields

I next employed the feature tracking method to produce velocity fields. From the two image pairs selected earlier, I produced two nonuniformly scattered vector fields over the Texas-Louisiana shelf, as shown in Figure 3a and Figure 3b. Flow in both images is highest in the area farthest away from the coast.

To properly use the feature tracking method, several precautions must be observed. If possible, use images 24 hours apart. A 24 hour lag between images filters diurnal and semidiurnal periodic motion and effects, factors such as tides and solar elevation. Before tracking

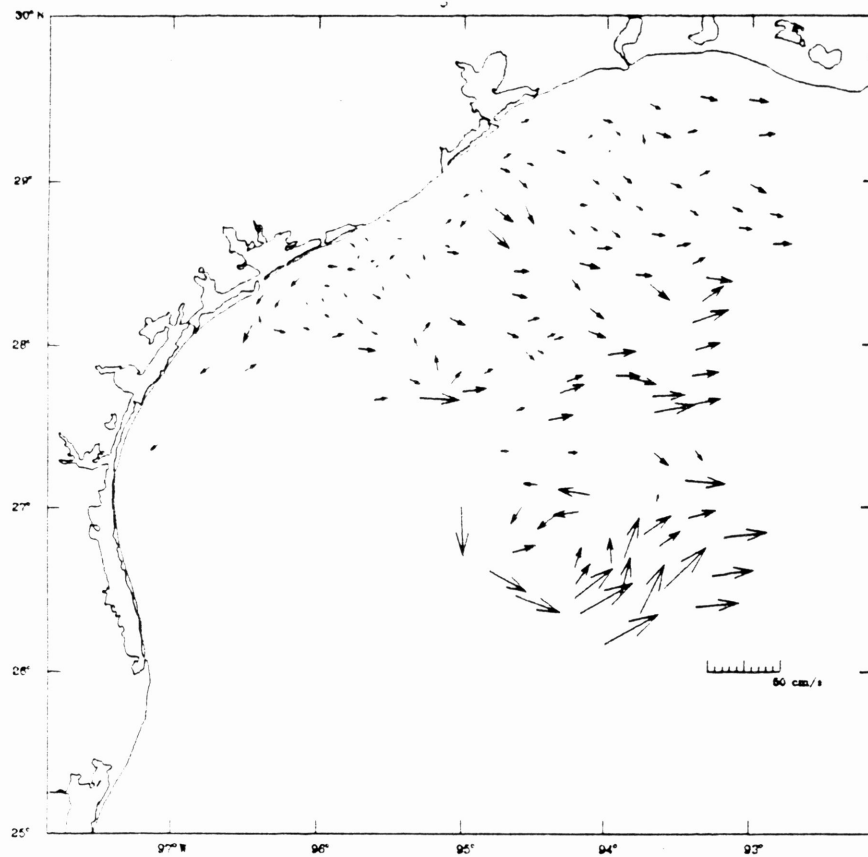


FIG. 3a. Vectors derived by AVHRR feature tracking between images of Julian days 69 (March 10) 14:23 and 70 (March 11) 14:00

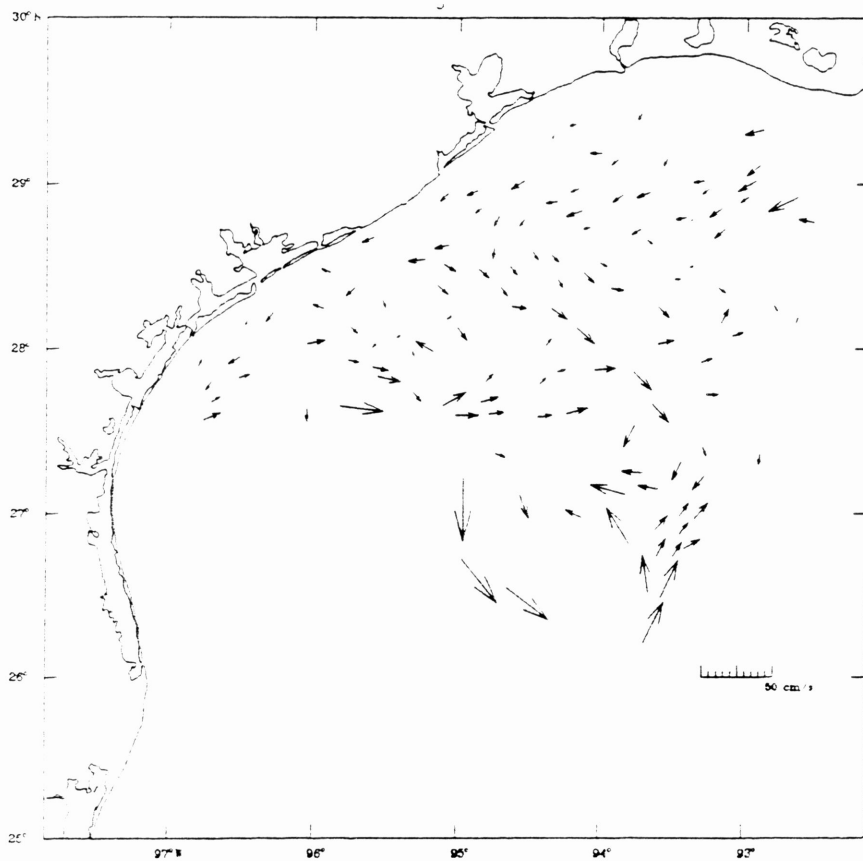


FIG. 3b. Vectors derived by AVHRR feature tracking between images of Julian days 70 (March 11) 08:47 and 71 (March 12) 08:37

individual features, study the changes between the images on a large scale. What may appear to be slow motion in one direction when viewed in a narrowly focused zoom may obviously be rapid motion in another direction when seen on a broader scale. Once the qualitative motion of a region is clear, zoom in more closely to carefully track the features. Since color is a function of the particular enhancement given to an image, avoid tracking color. Color changes between images may be due to heating or cooling rather than advection. A slight change in the enhancement will alter the apparent motion implied by color changes. When tracking features, investigate motion of distinct gradients first. These vectors can serve as guidelines for filling in more obscure areas of the field. Motion along fronts is easily followed, while small scale turbulence is difficult to represent.

#### SEA-TRUTHING

To sea-truth the buoy trajectories, I inserted model water parcels into the feature tracking vector fields at locations determined by the actual buoy trajectories. Each parcel was moved for 48 hours, and then the model trajectories were compared to the splines fit to the actual buoy positions. In practice, vector fields derived via feature tracking are used for periods of 24 hours or less, never for two days. Often, these vector fields are used to initiate sophisticated flow models which anticipate and account for changes in the flow pattern over time.

For each of the velocity fields I used two different model water parcel starting positions per buoy. The first starting position was the buoy location at the time of the first AVHRR image, while the second

starting position was the buoy position 12 hours earlier. Five parcels are included in each image to provide a broader picture of the flow field. A star marks the start of each track, a circle marks 00:00 GMT on the parcel tracks, and a square marks 00:00 GMT on the buoy track.

The first comparison of tracks uses the day 69:14 - 70:14 (March 10 14:37 to March 11 14:00) vector field. The parcels are started on March 10 at 14:00 and move for two days. Figures 4-6 illustrate the results. In the region about USCG 4571 I overestimated the toward the east, while in the region around USCG 4573 I underestimated the flow to the west. The track of USCG 4574 indicates a reversal in the flow field during the time of the vector image, an occurrence which can not be represented with these time-invariant fields.

Comparison with the day 70:08-71:08 (March 11 08:47 to March 12 08:37) vector field reveals closer correlation. Figures 7-9 indicate the results of parcels started on March 11 at 08:00. The parcel has close agreement with the buoy over the first day, with velocity still slightly overestimated toward the east. USCG 4573 is trapped in a small eddy, a feature poorly represented by the vector field. The water parcel remains fairly close over the first day, but because the field is time-invariant it travels in a direction opposite the buoy on the second day. The parcel follows USCG 4574 closely the over the first 24 hours, but fails to change with the buoy over the second 24 hours.

In an effort to minimize the effect of the time-invariant flow field, I next centered the flow field within the 48 hour test window. The parcel generally followed the buoy more closely than in the previous

two tests. Figures 10 and 11 reveal the product of the day 69:14 - 70:14 velocity vectors with parcels starting at 02:00 on March 10. The field still overestimates the flow toward the east around USCG 4571 and underestimates the flow toward the west around USCG 4573. USCG 4574 was not in the water at 02:00 on March 10.

Parcels started on March 10 at 20:00 show the strongest correlation with the buoy trajectories. Figures 12-14 show the tracks produced by the day 70:08 - 71:08 vector field. The parcels mirror USCG 4571 and USCG 4573 closely, and the parcel diverges from USCG 4574 only toward the end of the second 24 hour period.

#### RESULTS AND CONCLUSION

For each trial, I calculated the hourly error in the model track, the distance between the model parcel and the actual buoy after each hour time step. The results of the sea-truthing are depicted in Figures 15-18. Considering all trials, the rms error in position was 9.468 km after one day and 15.296 km after two days. Appendix B, Table B1 contains a more complete breakdown of the rms error.

The rms error varied considerably between different test cases. For parcels moved by the first field, the rms errors are 13.266 km after 24 hours and 19.640 km after 48 hours; in contrast, parcels moved by the second field have rms errors of only 4.203 km after 24 hours and 10.366 km after 48 hours. Parcels started at the same time as the first image have an rms error of 10.709 km after one day and 16.707 km after two. For parcels initiated 12 hours before the first image of the pair, rms errors were 7.331 km after 24 hours and 13.406 km after 48 hours.

The reliability the vector fields produced by the feature tracking method shows a high degree of variability between the two fields. The variability is probably a result of my inexperience with the parcel tracking method, rather than a fault of the method itself. Since the method is subjective, if I again derived vector fields from the same images I would probably get different results. I had more assistance and experience when I produced the second field; consequently, it consistently had lower rms errors. Results will improve as I become more proficient at tracking features.

The results also improve when the reference track is centered on the time midway between the images rather than started at the time of the first image. Since the field is time-invariant, extending the field beyond a single day produces unreliable results. Again the fault lies not with the feature tracking method but with the way the fields are used. Using a single field implies that the ocean is dynamically static, generally an invalid assumption. Results would improve if several fields were produced and combined into a time-dependent series. In practice, a velocity field derived from feature tracking is used only during the time spanned by the AVHRR images. More sophisticated models which are initialized by these velocity fields successfully represent the time evolution of the sea surface flow.

A third way to improve the results is to provide a more accurate velocity interpolation. The interpolator I used does not produce a smooth fit over the field, nor does it efficiently deal with very large numbers of vectors. Sparse data regions will be a problem for any interpolator, but some other methods might yield more reasonable

results. One option is to use the bivariate method to interpolate to a uniform grid and then to fit splines to cover the entire region. The field would then be smooth, and interpolation would be more efficient. Yet the resulting velocities would be farther removed from the original data. We need to find a better method of interpolation.

However, even with a more proficient feature tracker, time-dependent vector fields, and an improved interpolator, the correspondence between parcels moved by the vector field and drifting buoys will be imperfect. Errors are inherent in the satellite fixes on the buoy, in the brightness temperature values of the AVHRR images, in the navigation of the AVHRR images, in the tracking of thermal features, and in the integration of parcel motion. Oceanic motion is very complex, and motion on scales less than 1 km is invisible to the AVHRR images. The best we can hope for is to closely represent the motion on the scale of a few kilometers, a level possible with the AVHRR feature tracking method. Velocity fields produced by feature tracking seem best suited for large scale, qualitative descriptions of sea surface flow and for initialization of more sophisticated flow models which account for dynamic changes in the field.



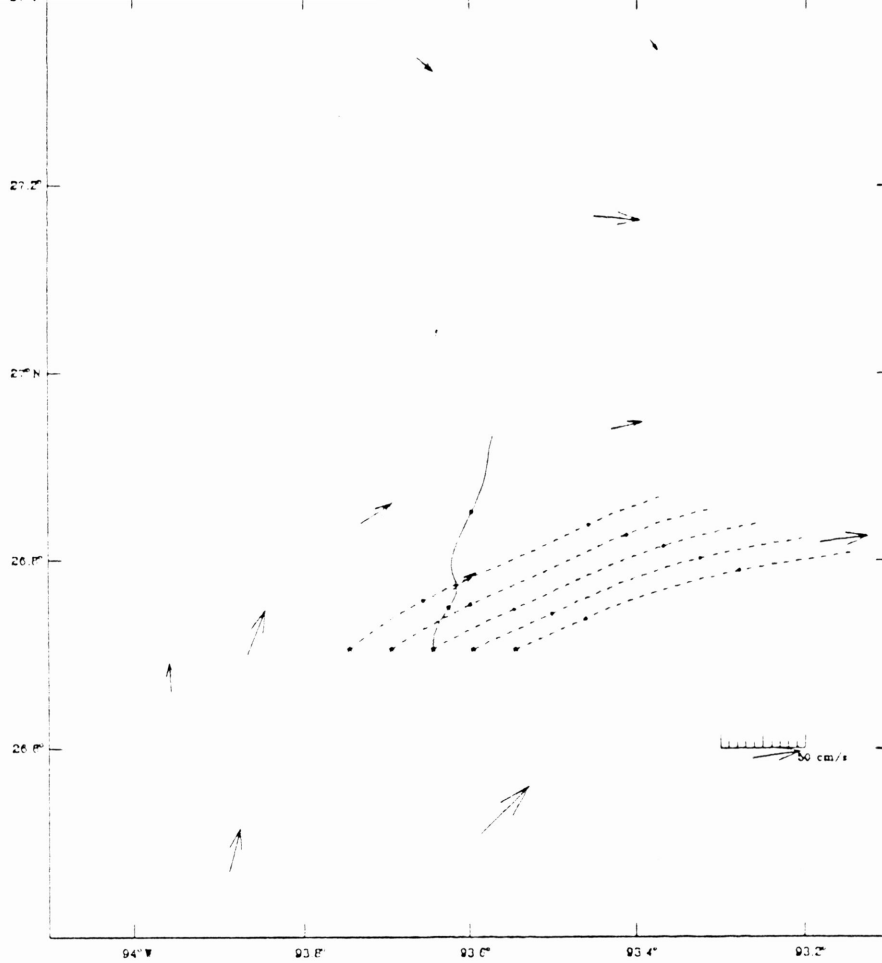


FIG. 4. Actual 2-day track of USCG\_4571 and 5 model parcels.  
 Vectors day 69:14 - 70:14. Parcels start day 69:14.

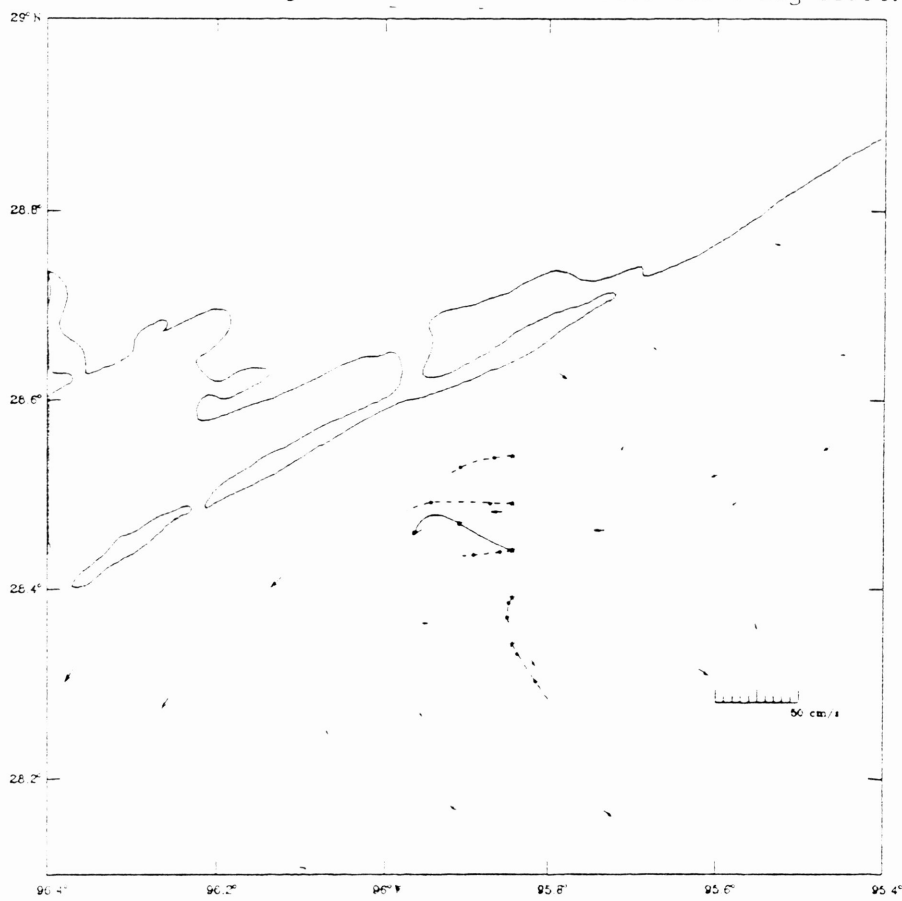


FIG. 5. Actual 2-day track of USCG\_4573 and 5 model parcels.  
 Vectors day 69:14 - 70:14. Parcels start day 69:14.

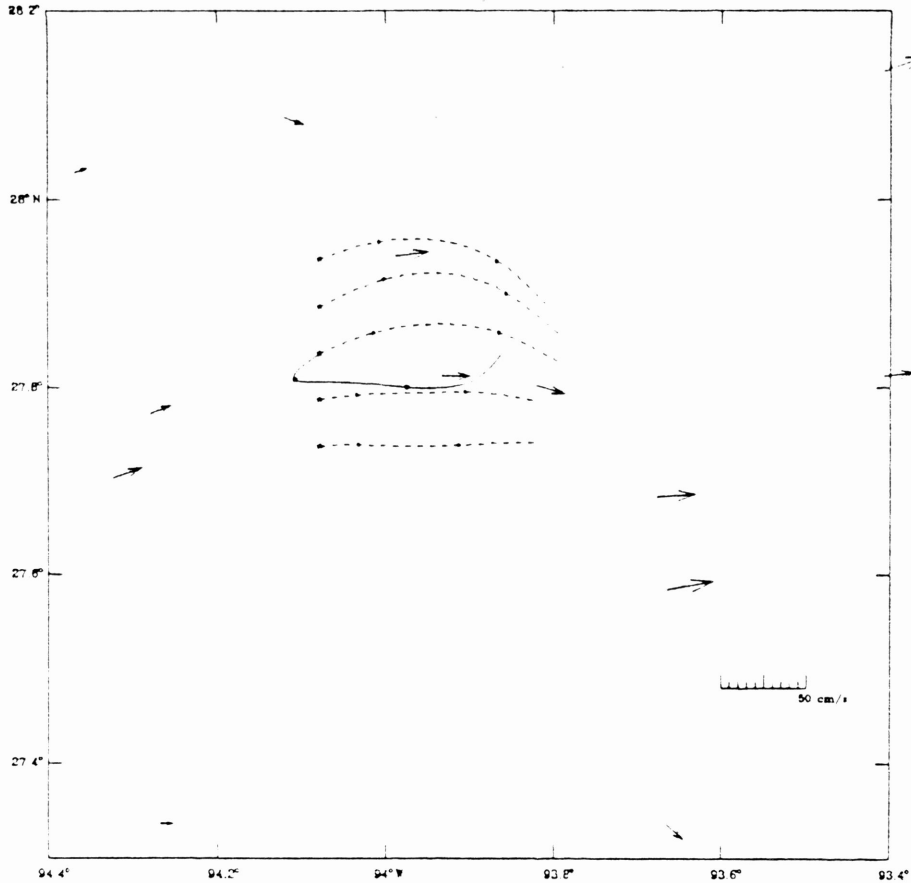


FIG. 6. Actual 2-day track of USCG\_4574 and 5 model parcels. Vectors day 69:14 - 70:14. Parcels start day 69:14.

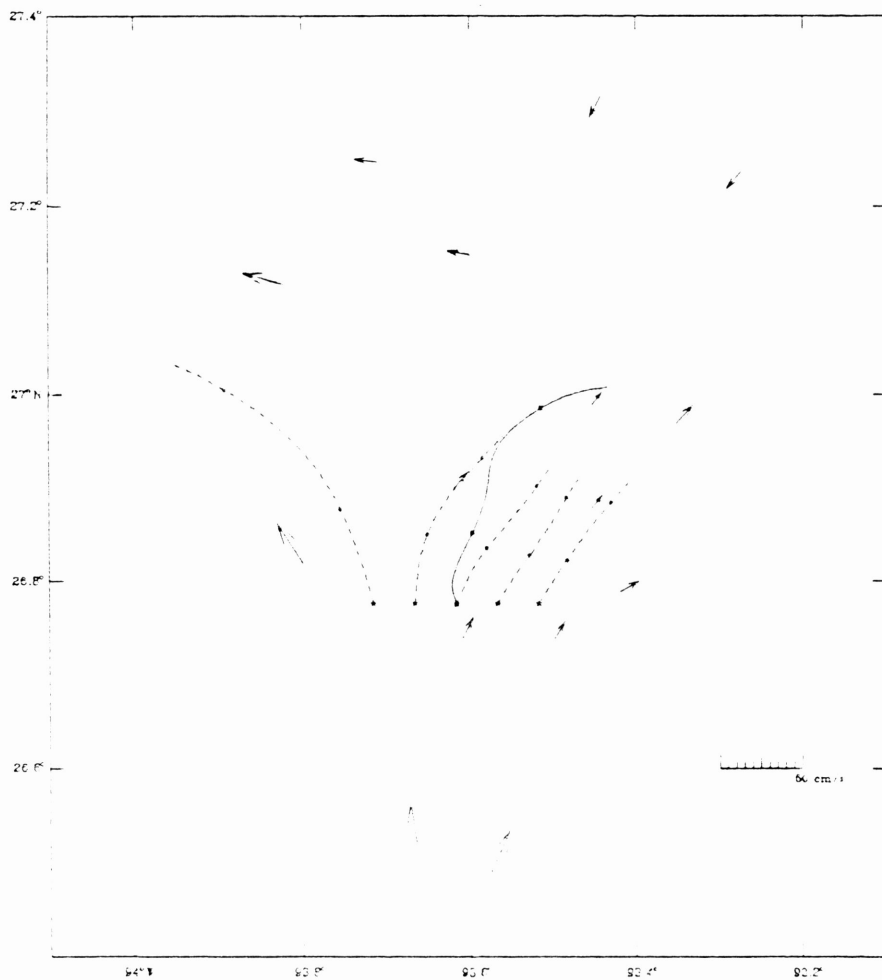


FIG. 7. Actual 2-day track of USCG\_4571 and 5 model parcels. Vectors day 70:08 - 71:08. Parcels start day 70:08.

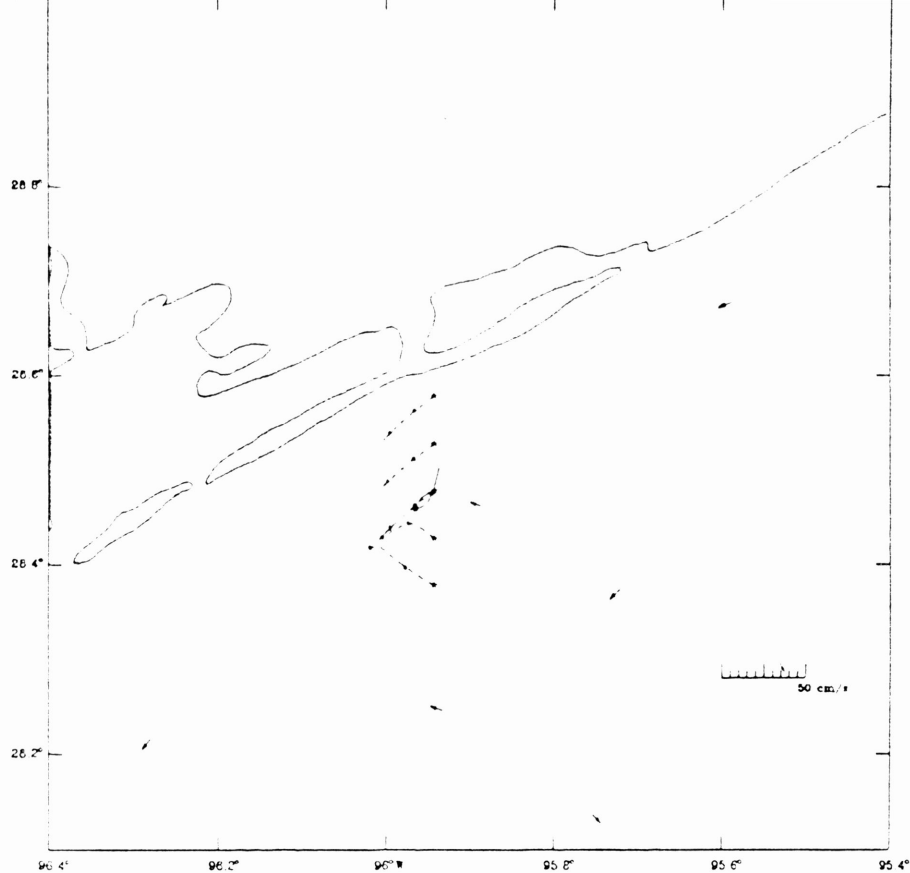


FIG. 8. Actual 2-day track of USCG\_4573 and 5 model parcels.  
 Vectors day 70:08 - 71:08. Parcels start day 70:08.

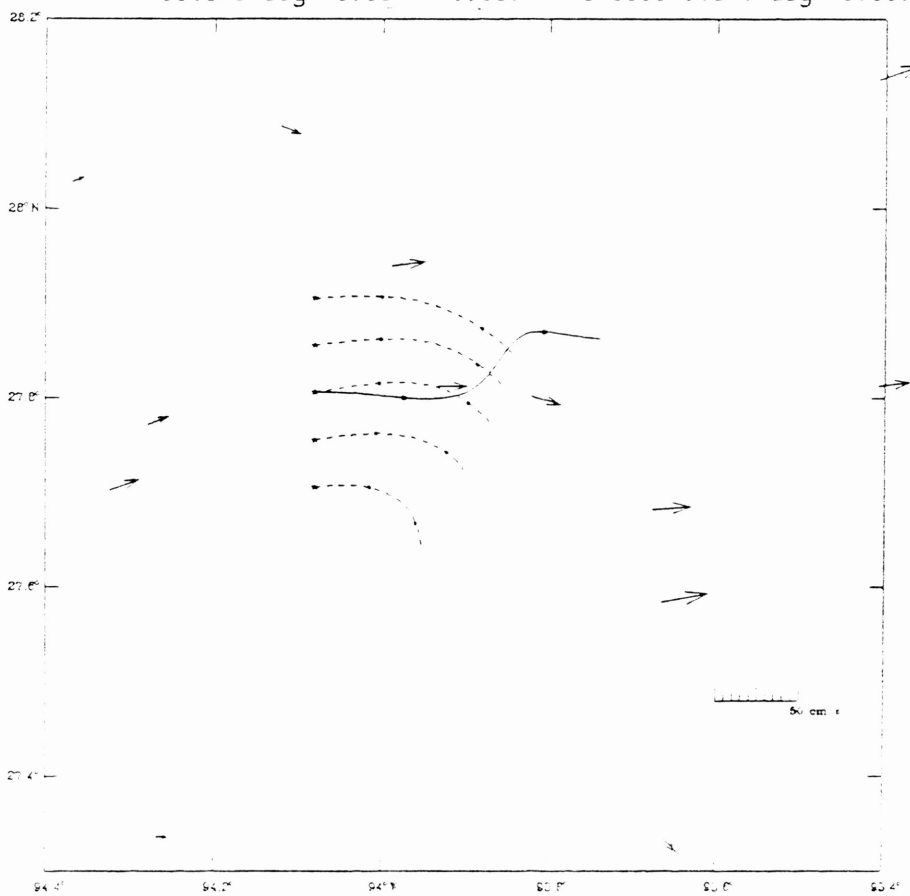


FIG. 9. Actual 2-day track of USCG\_4574 and 5 model parcels.  
 Vectors day 70:08 - 71:08. Parcels start day 70:08.

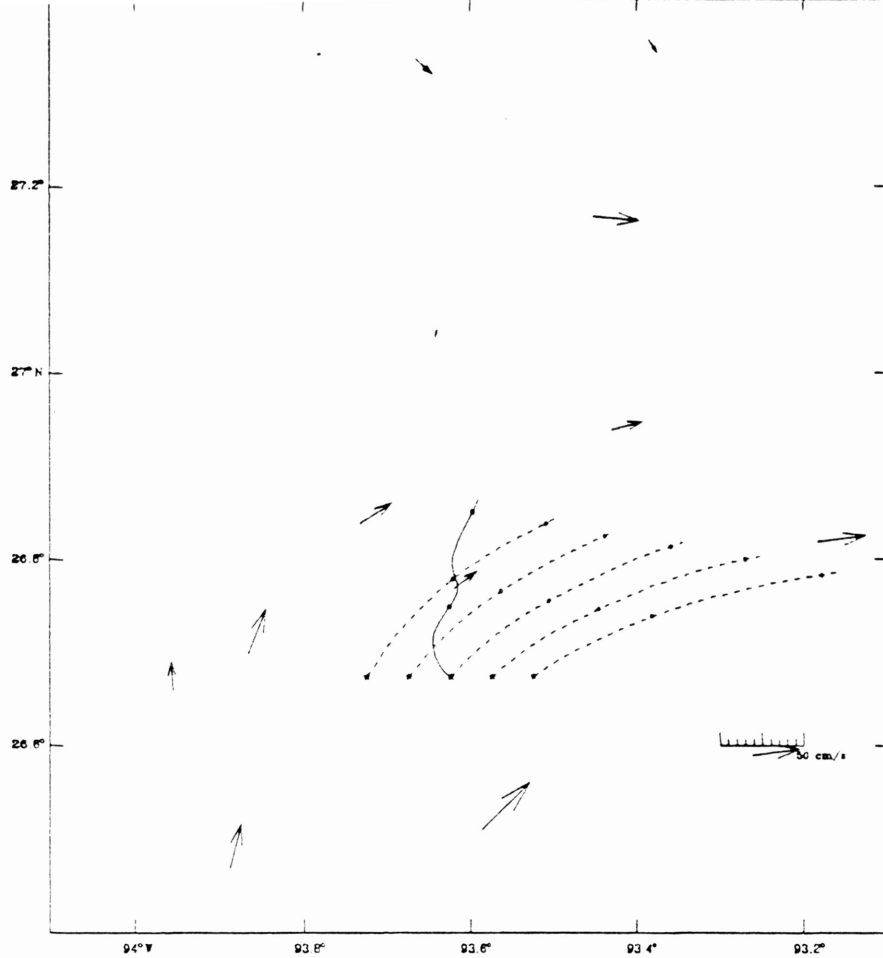


FIG. 10. Actual 2-day track of USCG\_4571 and 5 model parcels. Vectors day 69:14 - 70:14. Parcels start day 69:02.

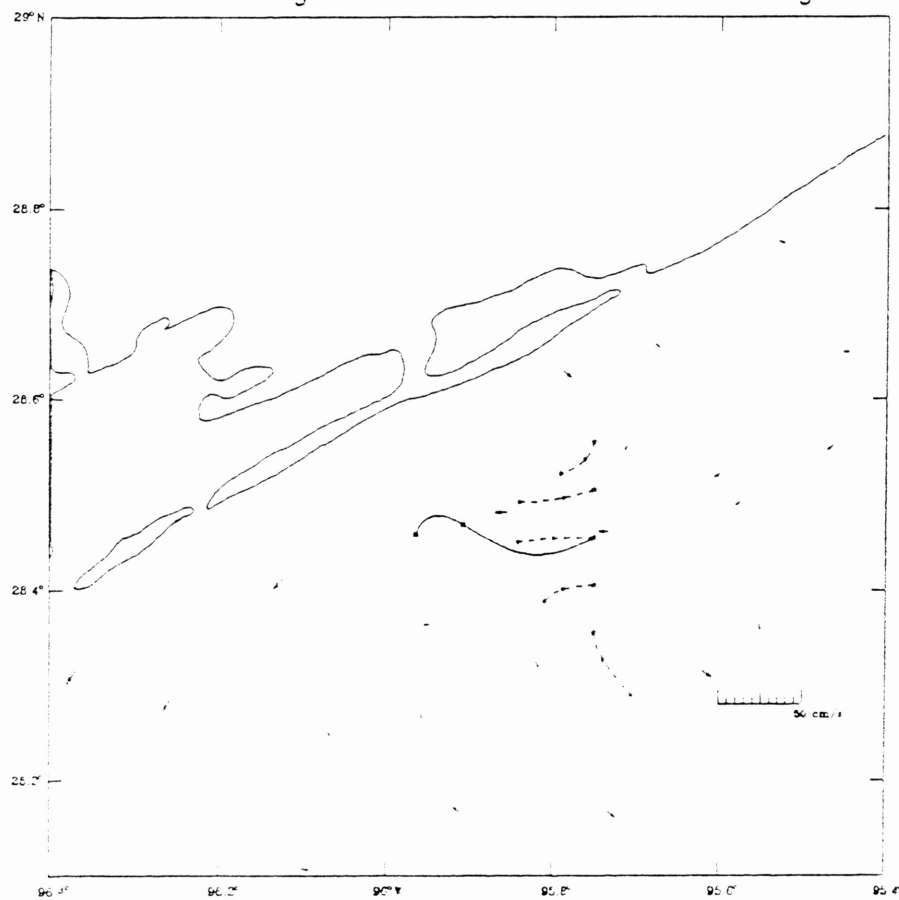


FIG. 11. Actual 2-day track of USCG\_4573 and 5 model parcels. Vectors day 69:14 - 70:14. Parcels start day 69:02.

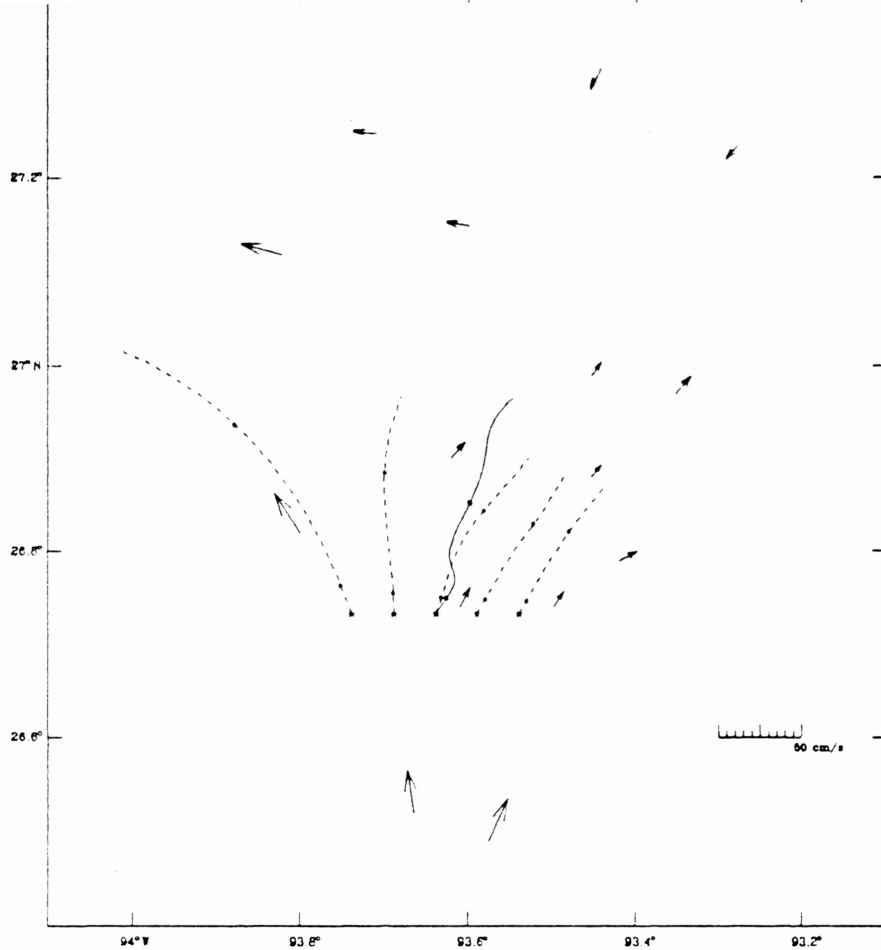


FIG. 12. Actual 2-day track of USCG\_4571 and 5 model parcels.  
 Vectors day 70:08 - 71:08. Parcels start day 69:20.

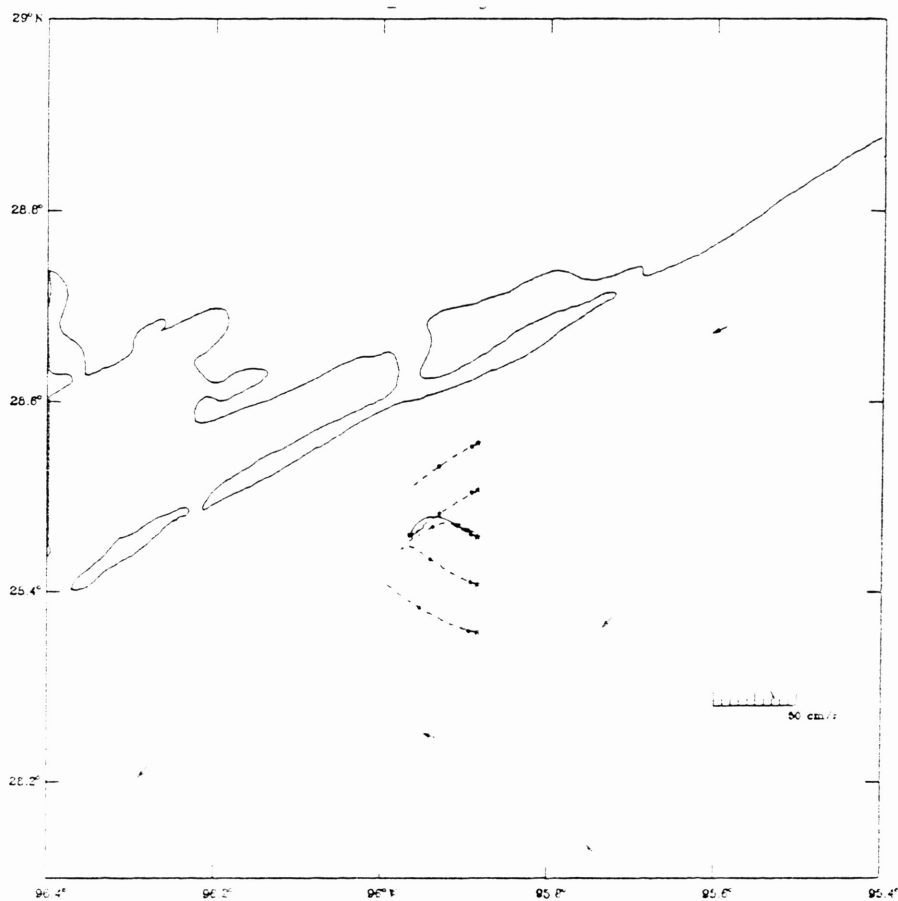


FIG. 13. Actual 2-day track of USCG\_4573 and 5 model parcels.  
 Vectors day 70:08 - 71:08. Parcels start day 69:20.

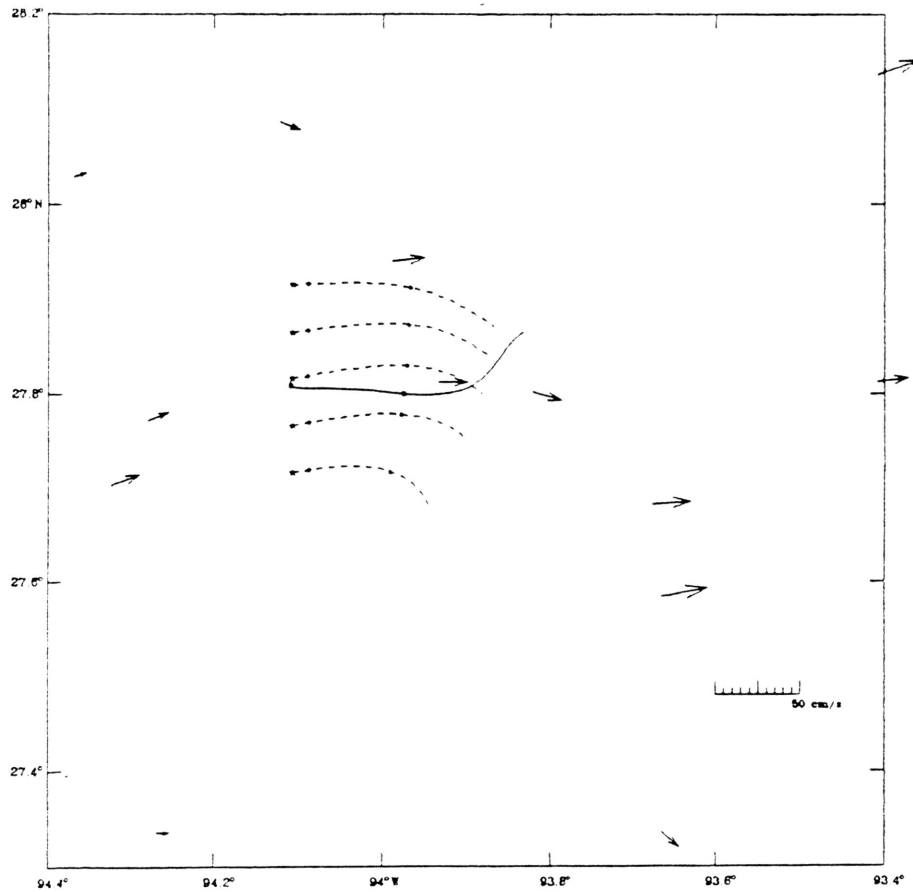


FIG. 14. Actual 2-day track of USCG\_4574 and 5 model parcels.  
Vectors day 70:08 - 71:08. Parcels start day 69:20.

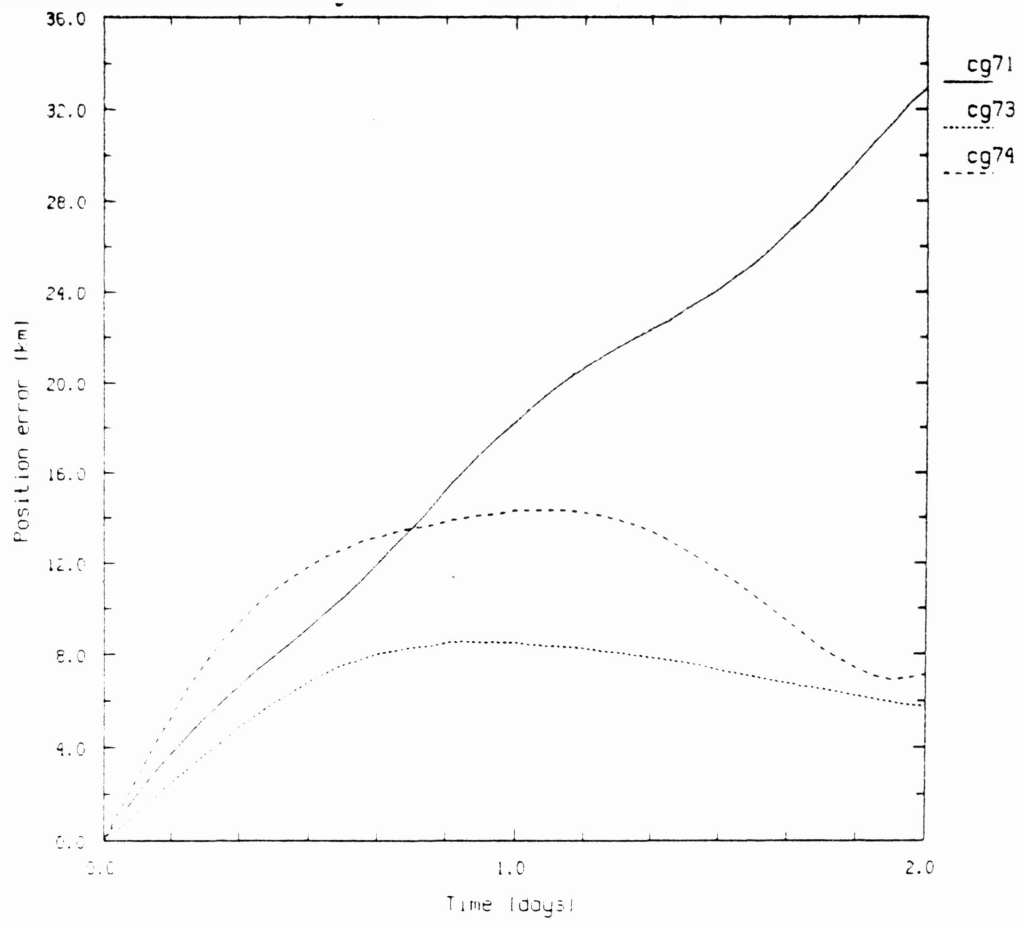


FIG. 15. Position difference between parcel and buoy vs. time. Vectors day 69:14 - 70:14. Parcels start day 69:14.

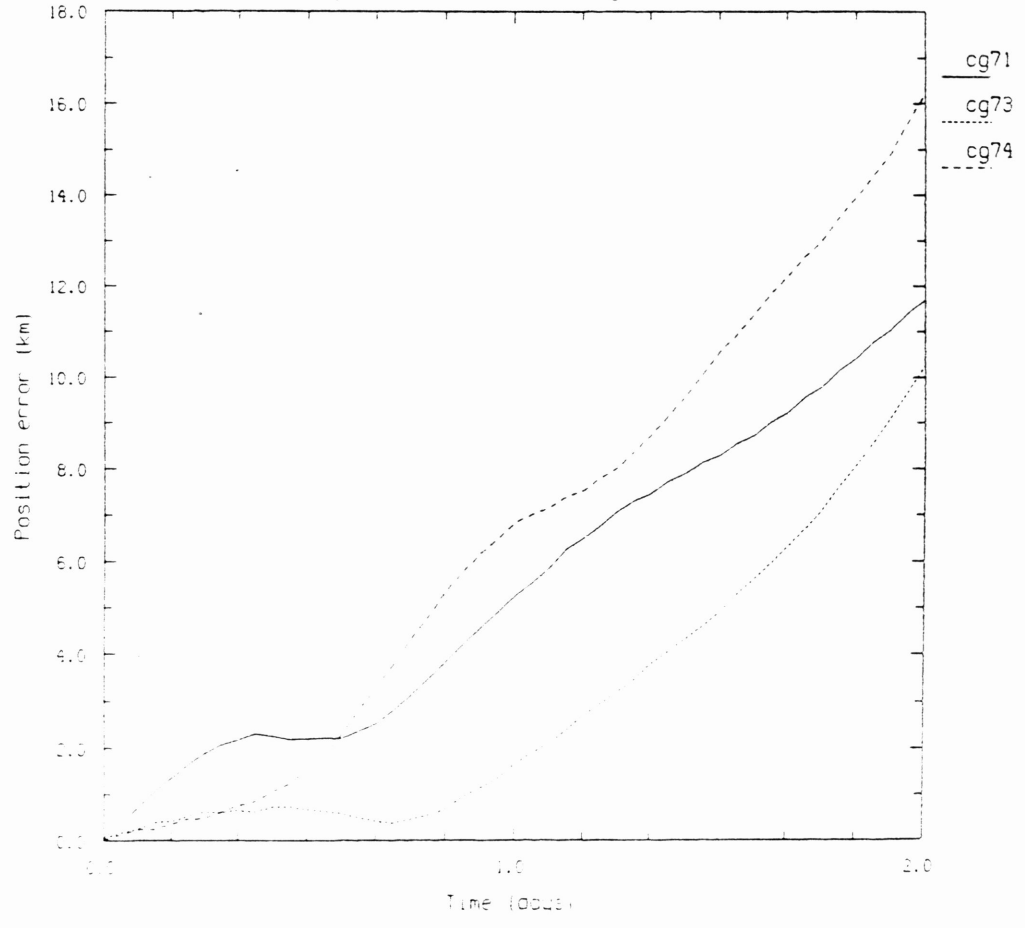


FIG. 16. Position difference between parcel and buoy vs. time. Vectors day 70:08 - 71:08. Parcels start day 70:08.

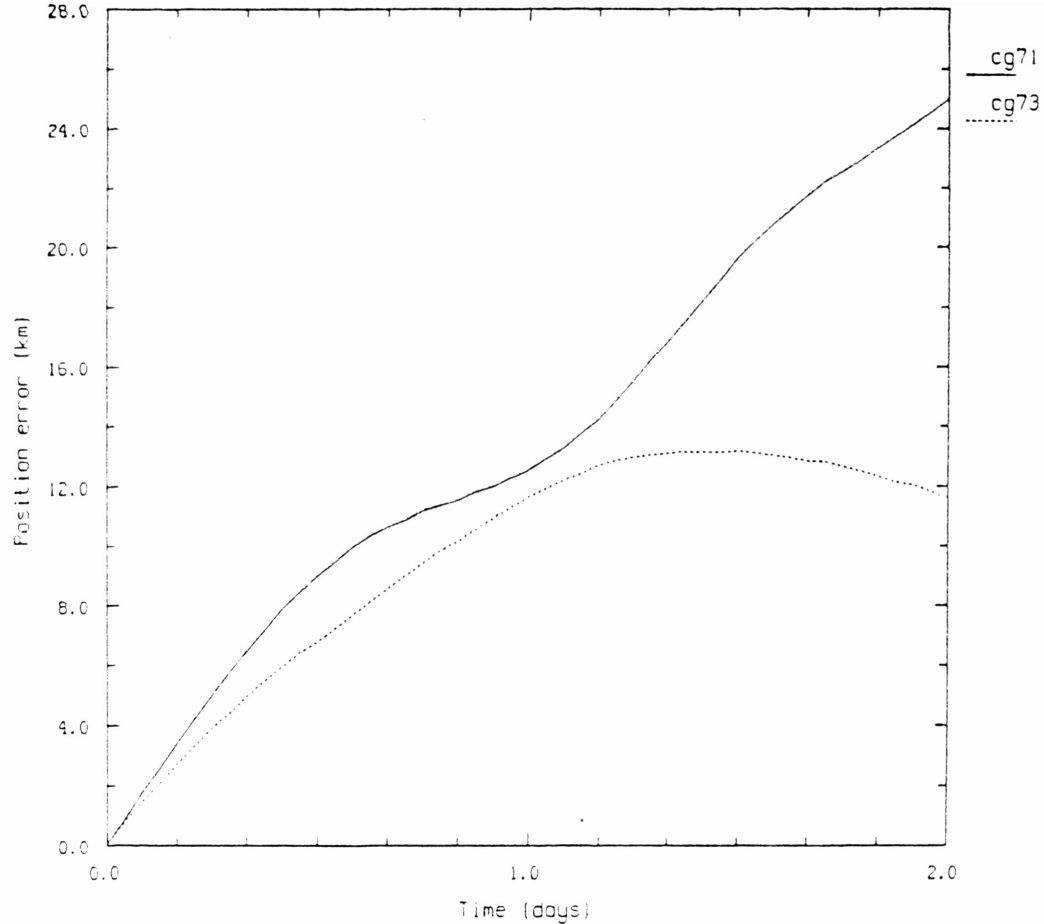


FIG. 17. Position difference between parcel and buoy vs. time.  
 Vectors day 69:14 - 70:14. Parcels start day 69:02.

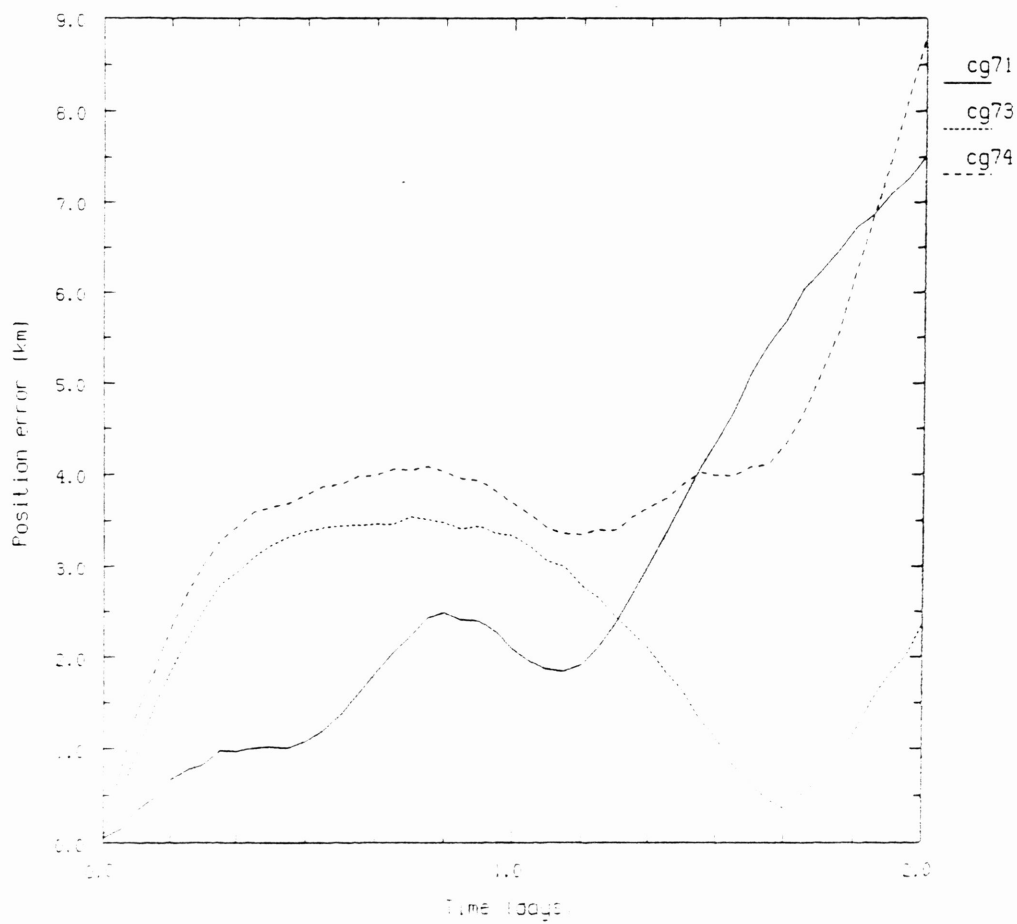


FIG. 18. Position difference between parcel and buoy vs. time.  
 Vectors day 70:08 - 71:08. Parcels start day 69:20.



## REFERENCES

- Akima, H. A Method of bivariate interpolation and smooth surface fitting for values given at irregularly distributed points. U.S. Dept. of Commerce/O. of Telecom., OT report 75-70, 1975.
- Eckart, C. Properties of sea water, part III. Amer. J. Sci., 256, 225-240, 1958.
- Emery, W. J., A. C. Thomas, M. J. Collins, W. R. Crawford and D. L. Mackas. An objective method for computing advective surface velocities from sequential infrared satellite images. J. Geophys. Res., 91, 12865-12878, 1986.
- Kelly, K. A. An inverse model for cross-isotherm velocity. Woods Hole Contribution No. 6768, submitted to J. Phys. Oceanogr., 1988.
- Molinari, R. L., D. W. Behringer, and J. F. Festa. Model studies of the circulation in the Gulf of Mexico. Final Report, BLM interagency agreement 08550-IA5-26, NOAA/AOML, Miami, FL, 244 pp., 1976.
- Press, W. H., B. P. Flannery, S. A. Teukolsky, and W. T. Vetterling. Numerical Recipes, 818 pp., Cambridge University Press, Cambridge, 1986.
- Vastano, A. C. and S. E. Borders. Sea surface motion over an anticyclonic eddy on the Oyashio Front. Remote Sens. Environ., 16, 87-90., 1984.
- Vastano, A. C. and R. O. Reid. Sea surface topography estimation with infrared satellite imagery. J. Atmos. Technol., 2, 393-400, 1985.
- Vukovich, F. M. Comparison of surface geostrophic currents calculated using satellite data and hydrographic data. Final Report, Research Triangle Institute, Research Triangle Park, NC, 27 pp., 1984.

## APPENDIX A

TABLE A1. Drifting buoy initial and final times and positions.

Buoy	Initial			Final		
	Date	GMT	Position	Date	GMT	Position
4571	Mar. 7	15:30	-93.831E,26.608N	Apr. 25	14:05	-96.369E,28.405N
4572	Mar. 7	07:56	-91.561E,27.033N	Apr. 27	07:39	-93.071E,29.373N
4573A	Mar. 7	19:17	-95.367E,28.661N	Mar. 13	19:53	-95.905E,28.548N
4573B	Mar. 25	13:53	-95.734E,27.839N	Apr. 27	07:39	-97.191E,27.637N
4574	Mar. 10	09:05	-94.048E,27.844N	Mar. 21	15:21	-93.381E,28.239N
4575	Mar. 12	07:03	-91.773E,28.313N	Apr. 20	01:57	-97.145E,26.340N
4576A	Mar. 11	18:37	-92.979E,29.053N	Mar. 28	20:46	-95.815E,28.662N
4576B	Apr. 22	01:10	-94.931E,27.496N	Apr. 29	20:18	-93.778E,28.278N

## APPENDIX B

TABLE B1. RMS distance between model parcels and actual buoys.

Hours after start	RMS Distance (kilometers)				
	All trials	Trials using 69:14 vectors	Trials using 70:08 vectors	Trials started at time of first image	Trials started 12 hours before first image
0	0.043	0.042	0.044	0.041	0.045
1	0.712	0.955	0.412	0.756	0.655
2	1.416	1.919	0.780	1.510	1.295
3	2.054	2.808	1.079	2.230	1.821
6	3.798	5.260	1.840	4.125	3.363
12	6.257	8.901	2.401	6.794	5.545
24	9.468	13.266	4.203	10.709	7.331
48	15.296	19.640	10.366	16.707	13.406